



OPEN

SUBJECT AREAS:

NANOPARTICLES

COORDINATION POLYMERS

SOLID-STATE CHEMISTRY

METAL-ORGANIC FRAMEWORKS

Ultrahigh Gas Storage both at Low and High Pressures in KOH-Activated Carbonized Porous Aromatic Frameworks

Yanqiang Li¹, Teng Ben^{2*}, Bingyao Zhang¹, Yao Fu¹ & Shilun Qiu^{1*}Received
10 May 2013Accepted
19 July 2013Published
13 August 2013

Correspondence and requests for materials should be addressed to T.B. (tben@jlu.edu.cn) or S.L.Q. (sqiu@jlu.edu.cn)

* These authors contributed equally to this work.

¹State Key Laboratory of Inorganic Synthesis & Preparation Chemistry, Jilin University, Changchun, China, ²Department of Chemistry, Jilin University, Changchun, China.

The carbonized PAF-1 derivatives formed by high-temperature KOH activation showed a unique bimodal microporous structure located at 0.6 nm and 1.2 nm and high surface area. These robust micropores were confirmed by nitrogen sorption experiment and high-resolution transmission electron microscopy (TEM). Carbon dioxide, methane and hydrogen sorption experiments indicated that these novel porous carbon materials have significant gas sorption abilities in both low-pressure and high-pressure environments. Moreover the methane storage ability of K-PAF-1-750 is among the best at 35 bars, and its low-pressure gas adsorption abilities are also comparable to the best porous materials in the world. Combined with excellent physicochemical stability, these materials are very promising for industrial applications such as carbon dioxide capture and high-density clean energy storage.

There is increasing evidence to suggest that microporous solids such as porous carbon, zeolite, porous organic-inorganic hybrid frameworks and porous organic polymer networks are excellent candidates for gas storage, recognition and separation¹⁻⁶. It is hoped that these materials might be applied to help solve the current global climate change and energy shortage crises, especially in relation to carbon dioxide capture and high-density hydrogen or methane storage. Many efforts have been made to develop new strategies and methods that target structures with much higher surface areas⁷⁻¹¹ and that also increase the binding intensity between framework and gases¹²⁻¹⁷. Unfortunately, there seems to be an irreconcilable contradiction between materials with an ultrahigh surface area and the interaction intensity between framework and gases. A more open structure, which is suitable for high-pressure gas storage applications, inevitably exhibits poor heat of adsorption (Q_{st}) and selectivity, which are unsuitable for gas adsorption in ambient conditions (1 bar and RT). It remains a great challenge to identify more convenient, effective methods for developing unique materials that share the properties of high heat adsorption to gases and a high surface area, which could be applied both in high-pressure gas storage and in ambient-condition gas sorption. Porous materials, especially porous carbons, have been investigated for several decades without losing its challenge and interest. Traditionally, porous carbons were obtained by physical or chemical activation of carbonaceous materials¹⁸. The commonly used activate agent can be CO₂, steam, KOH, ZnCl₂ and so on. With the development of zeolite and related porous materials, template method was developed to prepare porous carbon. Kyotani et al. pioneered this work¹⁹. Up to now, different types of zeolite such as zeolite Y, ZSM-5, LTA et al. have been used as template to synthesis porous carbon. The resulting zeolite-template carbons (ZTCs) show superior capacity for gas storage¹. Another important type of porous carbon called carbide-derived carbons (CDCs) was synthesized by selectively etching of metal atoms from metal carbides²⁰. CDCs exhibit ultra-micropore with very narrow pore distribution and high surface area. The pore characteristics make it very suitable for gas storage. For example, TiC-CDC could adsorb 336 cm³ g⁻¹ of H₂ at 77 K and 1 atm²¹. It should be noted that anomalous increase capacitance was observed in these microporous carbons²². Very recently, preparing porous carbons template or directly from Metal Organic Frameworks or porous coordination polymers (PCPs) emerged as a new strategy for porous carbon synthesis. Qiang Xu et al. first reported the synthesis porous carbon using MOF-5 as template, which showed high hydrogen uptake and capacitance²³. In 2011, Qiang Xu et al. reported another type of porous carbon using ZIF-8 as template, they showed the framework behaving as both a carbon precursor and a template, thus pave a new way to porous carbon²⁴. By direct carbonizing Al-PCP, Yusuke



Yamauchi got porous carbon with surface area as high as $5300 \text{ m}^2 \text{ g}^{-1}$ ²⁵. Heat treatments of porous polymers are also effective methods for preparation of advanced microporous materials. Kuhn et al. have observed microporous regular frameworks to mesoporous materials with ultrahigh surface area under heat treatment of nitriles in zinc chloride²⁶. Recently, Hauser et al. reported enhanced surface area of Yamamoto-derived porous organic polymers upon thermal treatment²⁷. Unlike heat treatment of porous polymer, our group proved that after direct carbonization of an ultrahigh surface area porous aromatic framework (PAF-1), the obtained microporous carbon show excellent carbon dioxide selectivity adsorption²⁸. PAF-1 combines the best physicochemical stability with an ultrahigh Brunauer-Emmett-Teller (BET) specific surface area of about $5640 \text{ m}^2 \text{ g}^{-1}$. Unfortunately, after carbonization, the BET surface area of PAF-1 derivatives decreased to about $1000 \text{ m}^2 \text{ g}^{-1}$, suggesting that these PAF-1 derivatives will exhibit less than excellent gas storage properties at high pressure. Recently, KOH was shown to activate porous carbon with high surface area and excellent gas storage properties^{29–31}. This prompted us to derive a suitable and convenient method for preparing advanced materials that have both high surface area and high heat of adsorption by chemical activation of PAF-1. Herein, we describe the preparation method for KOH-activated carbonized PAF-1 derivatives and the significant increases we observed in their gas uptake capacities under ambient conditions and their excellent high-pressure gas storage properties.

Results

The starting PAF-1 was synthesized using the optimized Yamamoto-type Ullmann cross-coupling method³². Arne Thomas et al. first applied this method to synthesize conjugated microporous polymer networks with surface area about $1275 \text{ m}^2 \text{ g}^{-1}$ ³³. The BET surface area of the fresh PAF-1 for this study was $5300 \text{ m}^2 \text{ g}^{-1}$, which is comparable to the originally reported PAF-1. Following the typical procedure, PAF-1 powder was first immersed into a KOH (PAF-1/KOH, 1/4, mass ratio) ethanol/water (95 : 5, v/v) solution and stirred overnight. The resulting mixture was distilled and the white residue was dried under vacuum. Carbonization was carried out by introducing the PAF-1/KOH powder mixture into a nickel crucible placed within a quartz tube furnace at a ramped rate of $2^\circ \text{C per min}^{-1}$, to a final temperature of between 500 and 900°C for 1 hour under ultrahigh pure N_2 (99.999%). After carbonization, the black residue was dropped into 2N HCl to remove excess KOH and salts and was further purified five times with deionized water, ethanol and chloroform. The resulting black powders were denoted as K-PAF-1-x, where x is the activation temperature (in $^\circ \text{C}$).

The pore structures of KOH-activated carbonized PAF-1 derivatives were explored in a nitrogen sorption experiment performed at 77 K from 0 to 1 atm after being fully degassed at 200°C under vacuum for 8 hours. The resulting isotherms (Figure 1A; also see supporting information, Figure S1A) of PAF-1 and all carbonized PAF-1 derivatives were type-1 isotherms that exhibited a sharp uptake in the low-pressure region (10^{-5} to 10^{-3} atm), which is a feature of microporous materials. This is also confirmed by the pore size distribution shown in Figure 1B (also see supporting information, Figure S1B). Similar to the behavior of many polymer networks, PAF-1 also showed a hysteresis loop, which is attributed to the swelling effects of soft material at a relative pressure of 0.2 to 0.8. This phenomenon disappeared in the KOH-activated carbonized PAF-1 derivatives, indicating that the rigidity of the framework increased and almost no “soft” part remained. Surprisingly, unlike the pore shrinking phenomena observed in direct carbonization of PAF-1²⁸, larger pores of 1.2 nm and smaller pores of less than 0.8 nm were observed.

As shown in Figure 2, K-PAF-1-600 showed an unexpectedly high carbon dioxide uptake capacity, with a value of $161 \text{ cm}^3 \text{ g}^{-1}$ at 273 K (equivalent to 24.0 wt%, 7.2 mmol g^{-1}). To the best of our knowledge, these values are the highest among all of the reported porous carbon materials and are comparable to the highest microporous solids reported that contain amine moieties to date^{34–36}. Importantly, K-PAF-1-600 showed completely reversible adsorption/desorption isotherms, which have rarely been observed in amine-modified porous solids because Q_{stCO_2} is too high, indicating unique physical capture/release properties. Flue gas from power plants usually contains about 15% CO_2 . Thus, CO_2 uptake capacity at about 0.15 bar is more relevant to post-combustion application. At 273 K and 0.15 bar, K-PAF-1-600 could adsorb $50 \text{ cm}^3 \text{ g}^{-1} \text{ CO}_2$ (2.2 mmol, 8.9 wt%). Although lower than Mg-MOF-74 and HKUST-1, this value is still comparable to that of PPN-6- SO_3Li and higher than many MOFs and KOH activated carbon^{4,37}. To further investigate the factors that affect the CO_2 uptakes of these carbonized PAF-1s, we measured the heat of adsorption of CO_2 . As expected, the Q_{stCO_2} of carbonized PAF-1 increased significantly from the original 15.6 kJ mol^{-1} in PAF-1 to 22.2 – 28.7 kJ mol^{-1} in KOH-activated carbonized PAF-1s (Table S3, Figure S2B). A CO_2 reversible adsorption (28°C) and regeneration (80°C) experiment was performed using a thermogravimetric analyzer under a carbon dioxide atmosphere at 1 bar. The K-PAF-1-600 underwent a significant average weight change of 8.4 wt% within the sorption and regeneration cycles (Figure 3). The difference between TGA and gravimetric measurement can be explained by the different adsorption process. For gravimetric measurement, the data was

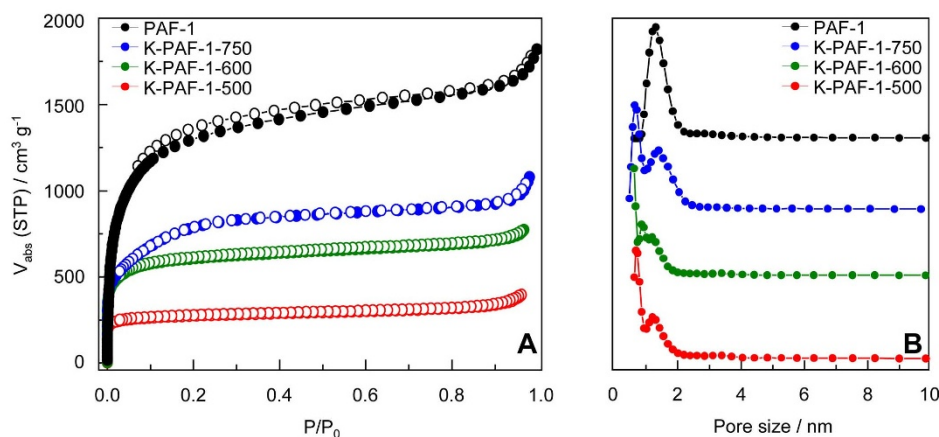


Figure 1 | (A) N_2 sorption isotherms (solid symbols, adsorption; open symbols, desorption) PAF-1 and KOH-activated carbonized PAF-1 derivatives at 77 K; (B) pore size distributions of PAF-1 and KOH-activated carbonized PAF-1 derivatives. The pore size distributions were calculated by the quench solid density functional theory (QSDFT) model.

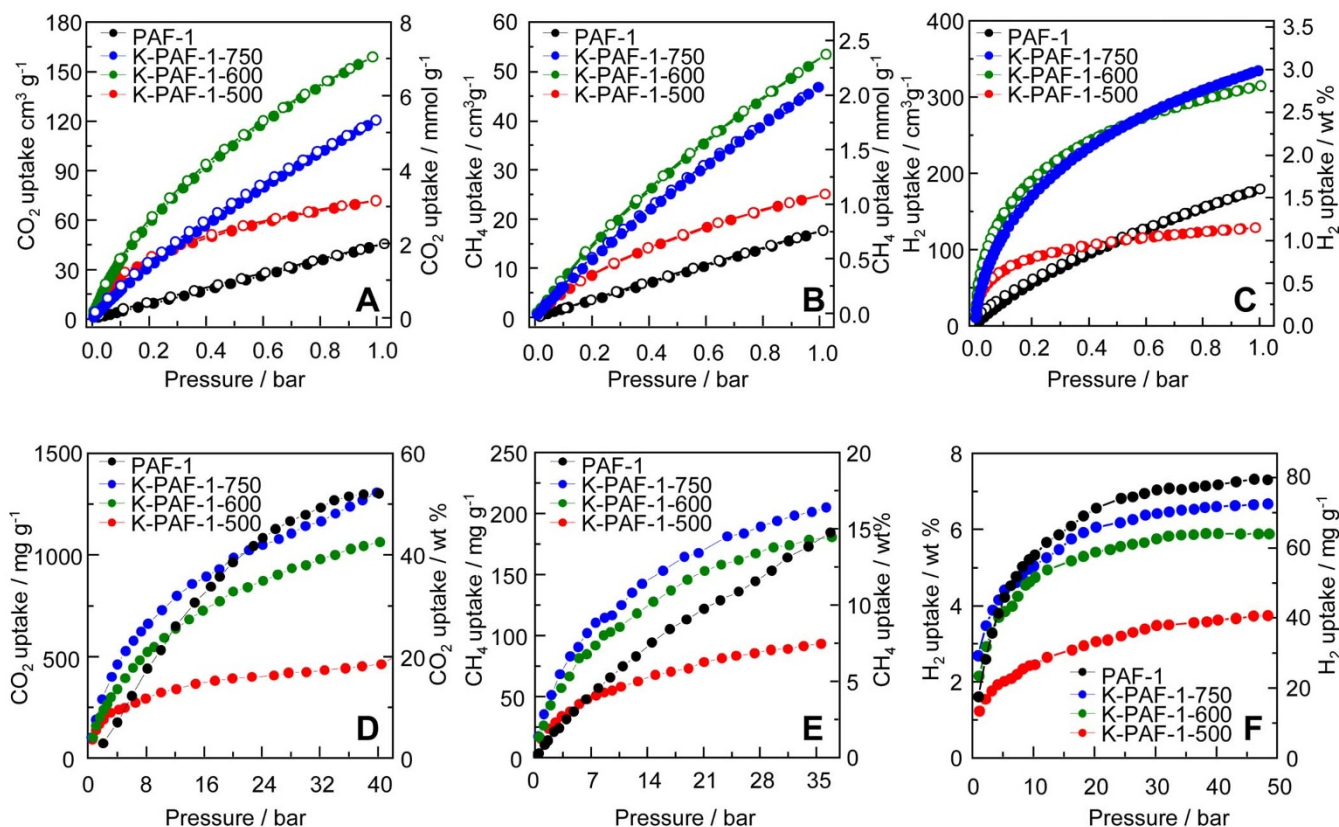


Figure 2 | (A) CO₂ uptake of PAF-1 and KOH-activated samples at 273 K and 1 bar; (B) CH₄ uptake of PAF-1 and KOH-activated samples at 273 K and 1 bar; (C) H₂ uptake of PAF-1 and KOH-activated samples at 77 K and 1 bar; (D) High-pressure CO₂ uptake of KOH-activated samples at 298 K; (E) High Pressure CH₄ uptake of KOH-activated samples at 298 K; (F) High-pressure H₂ uptake of KOH-activated samples at 77 K.

recorded at equilibrium condition. However, for TGA measurement, no equilibrium was achieved. Recently, Sheng Dai et al. reported nitrogen-doped carbonaceous adsorbents derived from task-specific ionic liquids which can absorb 15.5 wt% CO₂ by a different measurement using TGA³⁸. After ten cycles, no apparent loss of capacity was observed, suggesting completely reversible adsorption/desorption during each regeneration cycle. This result indicates that K-PAF-1-600 is a promising material for effective, reversible carbon dioxide capture. K-PAF-1-600 also showed very high methane uptakes of about 53.5 cm³ g⁻¹ at 1 bar, 273 K (2.4 mmol g⁻¹, 3.7 wt%),

Figure 2). Q_{stCH_4} ranged from 15.9–20.6 kJ mol⁻¹, higher than that of PAF-1 (Table S3, Figure S3B). Furthermore, using the ideal adsorption solution theory (IAST), the high selectivity of CO₂/N₂, CO₂/CH₄ and CO₂/H₂ were calculated as 81, 6.0, and 154 respectively (see supporting information, Figure S4). In terms of hydrogen adsorption ability at low pressure, K-PAF-1-750 exhibited the highest hydrogen uptakes of the KOH-activated PAF-1s, with a value of 342.2 cm³ g⁻¹ (15.3 mmol g⁻¹, 3.06 wt%) at 77 K, 1 bar (Table S3, Figure 2). This is the one of best hydrogen uptake material reported to date (Table S5)^{39,40}. The Q_{stH_2} of the carbonized derivatives was between 6.6–7.8 kJ mol⁻¹, which is also higher than that of PAF-1 (5.4 kJ mol⁻¹) (Table S3, Figure S5B). The successful high-pressure gas storage experiment also produced very exciting results. K-PAF-1-750 shared the highest BET surface area of these activated samples and showed the highest high-pressure gas storage abilities. Compared with PAF-1, K-PAF-1-750 is able to store 1320 mg g⁻¹ of carbon dioxide (56.9 wt%, 40 bar, RT), 207 mg g⁻¹ of methane (17.1 wt%, 35 bar, RT) and 71.6 mg g⁻¹ of hydrogen (6.68 wt%, 48 bar, 77 K) (Table S4, Figure 2, Figure S6–8). As predicted, the carbon dioxide and methane high-pressure storage ability surpassed the original PAF-1 (1.3 g g⁻¹ of carbon dioxide at 40 bar, 298K, 185 mg g⁻¹ of methane at 35 bar, 298K) and the hydrogen high-pressure storage was almost equal to that of PAF-1 (7.0 wt%, 48bar, 77K). It should be noted that K-PAF-1-750 is one of the best methane storage materials so far (Table S6). For natural gas storage, the United States Department of Energy (DOE) has put up a target for sorbents with volumetric and gravimetric capacities of 180 V_{CH₄} (STP)/V_{sorbent} and 0.5 g_{CH₄}/g_{sorbent} at reasonable temperature and pressures (−40°C–80°C and ≤35 bar). K-PAF-1-750 exhibit excellent methane storage ability about 0.207 g g⁻¹ at room temperature. Moreover, yet to our best knowledge, it is the first example that a material combines excellent gas uptakes both at high and low pressure.

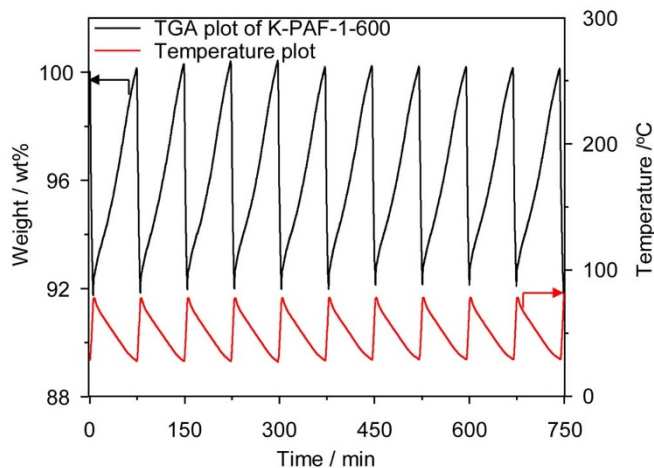


Figure 3 | CO₂ cyclic adsorption (28°C) and desorption (80°C) of K-PAF-1-600. The black curve shows the weight and the red curve is the temperature.



Similar to PAF-1, the KOH-activated carbonized PAF-1s possessed excellent thermal stability, which can be stable up to 400°C (5% weight loss, see supporting information, Figure S9). In addition, they were insoluble in common organic solvents such as alkanes, alcohols, acetones and DMFs and were very stable in cold conc. NaOH and HCl. These physicochemical stabilities are comparable to those of most activated carbon materials and are much better than those of many other porous materials.

Discussion

In our previous study of carbonization under a trace amount of oxygen, the BET surface area clearly decreased as the temperature increased, indicating pore collapse during carbonization²⁸. In this study, KOH was first adsorbed into the micropores of PAF-1. During carbonization, KOH acted not only as a chemical activating agent to produce new micropores, but also as a hard template to prevent the pores collapsing. The yield of carbonized PAF-1 decreased from 72.3% to 10.9% (see supporting information, Table S2), whereas the final temperatures increased. Fourier transform infrared spectroscopy (FTIR) was used to monitor the carbonization degree of porous carbon (see supporting information, Figure S10). The disappearance of C-H bands at 800 cm⁻¹ clearly indicated the elimination of hydrogen. The bands became broader and overlapping due to the strong adsorption of carbon-carbon bonds, particularly at heating temperatures above 600°C. The powder X-ray diffraction (PXRD) (see supporting information, Figure S11) results indicated that the carbonized PAFs were essentially amorphous. These results were consistent with the TEM images, in which a worm-like pore structure was observed (Figure 4, also see supporting information, Figure S12). The Raman spectra (see supporting information, Figure S13) of KOH-activated carbonized PAF-1 showed two Raman shifts, the G-band at 1580 cm⁻¹ is associated with the E_{2g} mode of graphite, whereas the D-band centered at around 1380 cm⁻¹ is attributed to the D-band of disordered carbon, corresponding to the defect-induced mode⁴¹. The intensity of the D-band to G-band ratio (I_D/I_G) was in the range of 0.70–0.90, indicating a low degree of graphitization.

To make sure of the elemental composition of K-PAF-1, we first perform the energy dispersive analysis of X-rays and results indicated

that no metal such as K remained in the framework after purification (See supporting information, Figure S14). Moreover, X-ray photoelectron spectroscopy (XPS) showed that only carbon and trace amount (<3%) oxygen were found on the surface. The presence of oxygen can be attributed to commonly observed surface contamination due to water adsorption in micropores^{42,43} (See supporting information, Figure S15). Thus, we proved that K-PAF-1 is composed of C and H. Furthermore, elemental analysis of these carbonized samples indicated that higher carbon/hydrogen ratio was obtained at higher annealing temperatures, attaining 98.34/1.66 at 800°C (see supporting information, Table S2).

According to the chemical activation mechanism⁴⁴, during the activation, the chemical reaction between KOH and carbons proceeds as $6\text{KOH} + 2\text{C} = 2\text{K} + 3\text{H}_2 + 2\text{K}_2\text{CO}_3$, followed by either decomposition of K₂CO₃ or the reaction of K/K₂CO₃/CO₂ with carbon. We thus attribute the smaller pores (0.6–0.8 nm) that were generated by KOH activation or pore shrinkage to carbonization at high temperature and the larger pores (1.2 nm) that originated from the PAF-1 itself, which were maintained during carbonization due to the hard template effect of the adsorbed KOH. Thus, the bimodal microporous structure was formed simply by KOH activation of PAF-1. The specific surface areas calculated BET models for relative pressures between 0.01 and 0.1 and the total pore volume calculated by the quenched solid density functional theory (QSDFT) models are listed in Table S2 (see supporting information). Consistent with previous results on the direct carbonization of PAF-1²⁸, the BET surface area dropped very quickly at 500°C, even when KOH-assisted. Interestingly, the BET surface areas and pore volumes clearly increased as the annealing temperature increased, reaching a threshold value of 2926 m² g⁻¹ and 1.14 cm³ g⁻¹ at 750°C. Due to the worm-like nature of the pore system, the diameter of the micropores could not be measured directly from the TEM images. However, the existence of the micropores and their worm-like structures of KOH-activated carbonized PAF-1s were confirmed by high-resolution TEM (Figure 4; also see supporting information, Figure S12). All the activated carbons exhibit a similar morphology that is characterized by irregular shaped particles with worm-like micropores. We could say that the larger micropores (1.2 nm) of original PAF-1 weren't destroyed by KOH activation at high temperature.

The above mentioned results reveal a series of bimodal KOH activated carbon materials were obtained and exhibit excellent gas sorption properties both at high pressure and low pressure. A key question is why this material is so unique among so many porous carbons? Recent studies have revealed that for gas adsorption at ambient temperatures, a pore size of less than 1 nm is preferable, commensurate with the kinetic diameter of gas molecules such as methane, hydrogen or carbon dioxide^{45–48}. Furthermore, larger pores (>1 nm) are always observed in porous solids that share the highest surface area and gas uptake capacities at high pressure (see supporting information, Table S7). Generally, the ultrahigh surface area materials applied in high-pressure gas storage show poor heat of adsorption to gases, which makes them unsuitable for ambient condition gas adsorption. Fortunately, through KOH activation, the carbonized PAF-1 derivatives showed a high BET surface area and a bimodal micropore structure with pores located at 1.2 nm and 0.6–0.8 nm, and had the potential to exhibit excellent gas adsorption properties both in high-pressure and ambient conditions. Though sometimes bimodal micropore structure could be also found in some reported microporous carbon^{49,50}, we believe K-PAF-1 is unique because we cannot ignore the function of starting PAF-1. TEM and nitrogen adsorption results indicated that the pore size distribution of original PAF-1 is not completely destroyed by KOH activation which makes it different with microporous carbon material activated by other carbon source. More accurate micropore analysis of K-PAF-1 revealed that different composition of microporosity of smaller pores (0.6–0.8) and larger micropore of 1.2 nm may also play

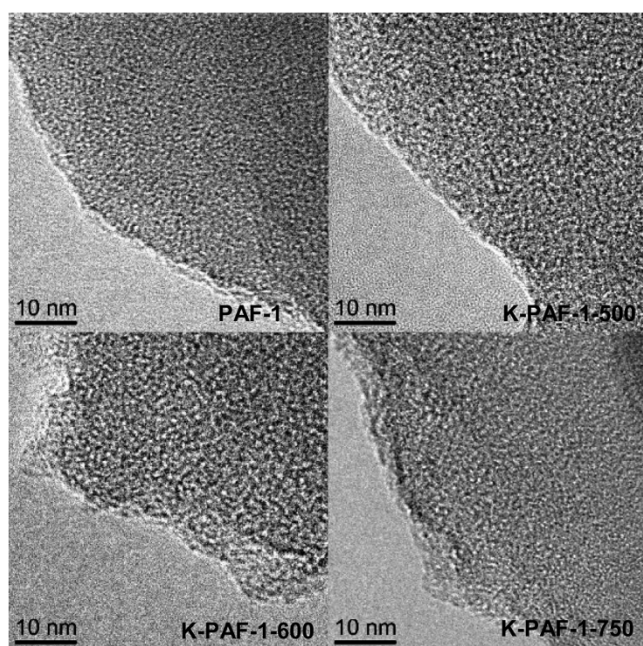


Figure 4 | TEM images of (A) PAF-1 and (B–D) samples activated with KOH at 500°C, 600°C and 750°C, respectively.

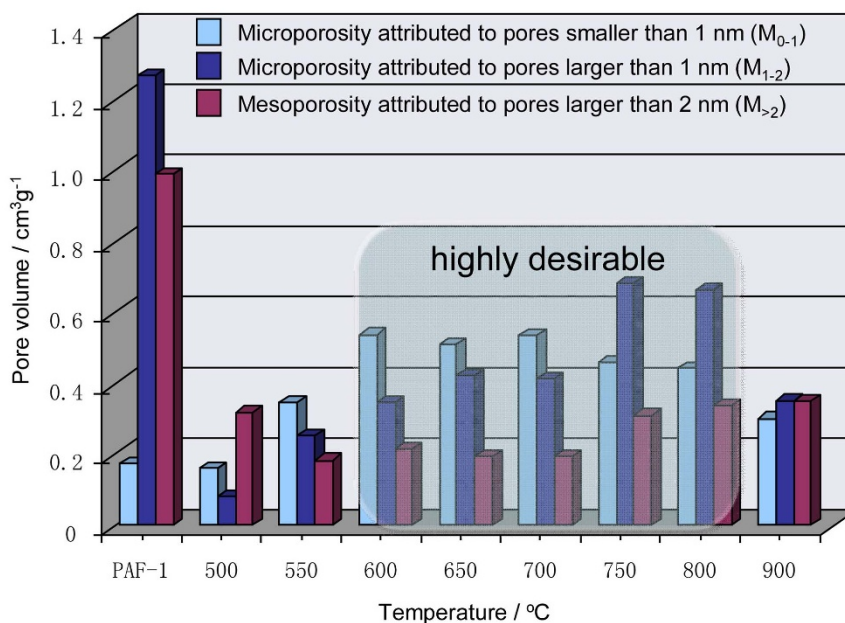


Figure 5 | Pore volume analysis of PAF-1 and KOH activated PAF-1.

an important role. Microporosity (in term of pore volume) attributed to pores smaller than 1 nm (M_{0-1} for short), microporosity attributed to pores about 1.2 nm (M_{1-2} for short) and mesopore ($M_{>2}$ for short) were shown in Figure 5 (also see supporting information, Table S8). The starting PAF-1 has very high M_{1-2} and exhibits very excellent high pressure gas storage abilities while its M_{0-1} is low and shows poor low pressure gas sorption ability. K-PAF-1-600, K-PAF-1-650, K-PAF-1-700, K-PAF-1-750, K-PAF-1-800 show both very high ($>0.3 \text{ cm}^3 \text{ g}^{-1}$) M_{0-1} and M_{1-2} and the cooperation effect of these two kinds of pores result in excellent gas sorption both at high pressure and low pressure. Another fact is after carbonization, the mesopore shrunk (about $0.2 \text{ cm}^3 \text{ g}^{-1}$, far less than that of PAF-1), which is coincided with our previously results²⁸. Furthermore, stronger interactions between the carbonized PAF-1s are desirable because all-carbon-scaffold networks can be expected to create strong polarity on the frameworks' surface, which imparts the networks with a strong affinity toward gases molecules such as hydrogen, methane and carbon dioxide through their high quadrupole moments. In sum, as indicated in Table S3 and Table S4 (also see supporting information, Figure S2–8), KOH-activated PAF-1s exhibit higher uptake of carbon dioxide, methane and hydrogen than PAF-1 at both low pressure and high pressure due to the cooperative of special bimodal micropores and polarized all-carbon-scaffold networks.

In conclusion, we developed a new method of carbonization of microporous polymer to obtain new class of microporous carbon. The carbonized PAF-1 derivatives formed by high-temperature KOH activation showed a special bimodal microporous structure located at 0.6 nm and 1.2 nm and a high surface area. These robust microporous structures were confirmed by nitrogen sorption experiment. Carbon dioxide, methane and hydrogen sorption experiments indicated that these novel porous carbon materials have significant gas sorption abilities in both low-pressure and high-pressure environments. Moreover the methane storage ability of K-PAF-1-750 is among the best at 35 bar, and its low-pressure gas adsorption abilities are also comparable to the best porous materials in the world, showing a world record low-pressure hydrogen capacity. So far, it is the first example that a material combined ultrahigh gas storage both at high and low pressure. Combined with excellent physicochemical stability, these materials are very promising for industrial applications such as carbon dioxide capture and high-density clean energy

storage. Pore size design and targeted preparation by chemical activation of carbonized PAFs represent a novel method for developing advanced microporous materials, and this novel area is worth exploring deeper.

Methods

Sample preparation: PAF-1 was synthesized according to our previous report¹¹. In a typical procedure, PAF-1 powder was first immersed into a KOH (PAF-1/KOH, 1/4, mass ratio) ethanol/water (95:5, v/v) solution and stirred overnight. The resulting mixture was distilled and the white residue was dried under vacuum. Carbonization was carried out by introducing a PAF-1/KOH powder mixture into a nickel crucible placed within a quartz tube furnace at a ramped rate of 2°C min^{-1} to a final temperature of between 500 and 900 °C for 1 hour under ultrahigh pure N_2 (99.999%). After carbonization, the black residue was dropped into 2N HCl to remove excess KOH and salts, and was further purified five times with deionised water, ethanol and chloroform. The resulting black powders were denoted as K-PAF-1-x, where x is the activation temperature (in °C).

- Nishihara, H. & Kyotani, T. Templated Nanocarbons for Energy Storage. *Adv. Mater.* **24**, 4473–4498 (2012).
- Morris, R. E. & Wheatley, P. S. Gas Storage in Nanoporous Materials. *Angew. Chem. Int. Ed.* **47**, 4966–4981 (2008).
- Suh, M. P., Park, H. J., Prasad, T. K. & Lim, D. W. Hydrogen Storage in Metal-Organic Frameworks. *Chem. Rev.* **112**, 782–835 (2012).
- Sumida, K. *et al.* Carbon Dioxide Capture in Metal-Organic Frameworks. *Chem. Rev.* **112**, 724–781 (2012).
- Li, J. R., Sculley, J. & Zhou, H. C. Metal-Organic Frameworks for Separations. *Chem. Rev.* **112**, 869–932 (2012).
- Dawson, R. *et al.* Microporous Organic Polymers for Carbon Dioxide Capture. *Energy Environ. Sci.* **4**, 4239–4245 (2011).
- Farha, O. K. *et al.* Metal–Organic Framework Materials with Ultrahigh Surface Areas: Is the Sky the Limit? *J. Am. Chem. Soc.* **134**, 15016–15021 (2012).
- Yuan, D. Q., Lu, W. Q., Zhao, D. & Zhou, H. C. Highly Stable Porous Polymer Networks with Exceptionally High Gas-Uptake Capacities. *Adv. Mater.* **23**, 3723–3725 (2011).
- Furukawa, H. *et al.* Ultrahigh Porosity in Metal-Organic Frameworks. *Science*. **329**, 424–428 (2010).
- Farha, O. K. *et al.* De Novo Synthesis of a Metal–Organic Framework Material Featuring Ultra-High Surface Area and Gas Storage Capacities. *Nat. Chem.* **2**, 944–948 (2010).
- Ben, T. *et al.* Targeted Synthesis of a Porous Aromatic Framework with High Stability and Exceptionally High Surface Area. *Angew. Chem. Int. Ed.* **48**, 9457–9460 (2009).
- Murray, L. J., Dinca, M. & Long, J. R. Hydrogen storage in metal–organic frameworks. *Chem. Soc. Rev.* **38**, 1294–1314 (2009).
- Bae, Y.-S. *et al.* Carborane-based metal–organic frameworks as highly selective sorbents for CO_2 over methane. *Chem. Commun.* 4135–4137 (2008).



14. Sun, D. F., Ma, S. Q., Ke, Y. X., Collins, D. J. & Zhou, H. C. An Interweaving MOF with High Hydrogen Uptake. *J. Am. Chem. Soc.* **128**, 3896–3897 (2006).
15. Nour, F. *et al.* Supermolecular Building Blocks (SBBs) for the Design and Synthesis of Highly Porous Metal–Organic Frameworks. *J. Am. Chem. Soc.* **130**, 1833–1835 (2008).
16. Phan, A. *et al.* Synthesis, Structure, and Carbon Dioxide Capture Properties of Zeolitic Imidazolate Frameworks. *Acc. Chem. Res.* **43**, 58–67 (2010).
17. Banerjee, R. *et al.* Control of Pore Size and Functionality in Isoreticular Zeolitic Imidazolate Frameworks and their Carbon Dioxide Selective Capture Properties. *J. Am. Chem. Soc.* **131**, 3875–3877 (2009).
18. Wang, H., Gao, Q. & Hu, J. High Hydrogen Storage Capacity of Porous Carbons Prepared by Using Activated Carbon. *J. Am. Chem. Soc.* **131**, 7016–7022 (2009).
19. Ma, Z., Kyotani, T., Liu, Z., Terasaki, O. & Tomita, A. Very High Surface Area Microporous Carbon with A Three-dimensional Nano- array Structure: Synthesis and Its Molecular Structure. *Chem. Mater.* **13**, 4413–4415 (2001).
20. Gogotsi, Y. *et al.* Nanoporous Carbide-Derived Carbon with Tunable Pore Size. *Nature Materials*. **2**, 591–594 (2003).
21. Yushin, G., Dash, R., Jagiello, J., Fischer, J. E. & Gogotsi, Y. Carbide- Derived Carbons: Effect of Pore Size on Hydrogen Uptake and Heat of Adsorption. *Adv. Funct. Mater.* **16**, 2288–2293 (2006).
22. Chmiola, J. *et al.* Anomalous Increase in Carbon Capacitance at Pore Sizes Less Than 1 Nanometer. *Science*. **313**, 1760–1763 (2006).
23. Liu, B., Shioyama, H., Akita, T. & Xu, Q. Metal–Organic Framework as a Template for Porous Carbon Synthesis. *J. Am. Chem. Soc.* **130**, 5390–5391 (2008).
24. Jiang, H.-L. *et al.* From Meatal–Organic Framework to Nanoporous Carbon: Toward a Very High Surface Area and Hydrogen Uptake. *J. Am. Chem. Soc.* **133**, 11854–11857 (2011).
25. Hu, M. *et al.* Direct Carbonization of Al-Based Porous Coordination Polymer for Synthesis of Nanoporous Carbon. *J. Am. Chem. Soc.* **134**, 2864–2867 (2012).
26. Kuhn, P., Forget, A., Su, D. S., Thomas, A. & Antonietti, M. From Microporous Regular Frameworks to Mesoporous Materials with Ultrahigh Surface Area: Dynamic Reorganization of Porous Polymer Networks. *J. Am. Chem. Soc.* **130**, 13333–13337 (2008).
27. Hauser, B. G., Farha, O. K., Exley, J. & Hupp, J. T. Thermally Enhancing the Surface Area of Yamamoto-Derived Porous Organic Polymers. *Chem. Mater.* **25**, 12–16 (2013).
28. Ben, T. *et al.* Selective adsorption of carbon dioxide by carbonized porous aromatic framework (PAF). *Energy Environ. Sci.* **5**, 8370–8376 (2012).
29. Sevilla, M., Valle-Vigón, P. & Fuertes, A. B. N-Doped Polypyrrole-Based Porous Carbons for CO₂ Capture. *Adv. Funct. Mater.* **21**, 2781–2787 (2011).
30. Srinivas, G., Burress, J. & Yildirim, T. Graphene oxide derived carbons (GODCs): synthesis and gas adsorption properties. *Energy Environ. Sci.* **5**, 6453–6459 (2012).
31. Hilton, R. *et al.* Mass Balance and Performance Analysis of Potassium Hydroxide Activated Carbon. *Ind. Eng. Chem. Res.* **51**, 9129–9135 (2012).
32. Yamamoto, T. π -Conjugated Polymers Bearing Electronic and Optical Functionalities. Preparation by Organometallic Polycondensations, Properties, and Their Applications. *Bull. Chem. Soc. Jpn.* **72**, 621–638 (1999).
33. Schmidt, J., Werner, M. & Thomas, A. Conjugated Microporous Polymer Networks via Yamamoto Polymerization. *Macromolecules* **42**, 4426–4429 (2009).
34. An, J., Geib, S. J. & Rosi, N. L. High and Selective CO₂ Uptake in a Cobalt Adeninate Metal–Organic Framework Exhibiting Pyrimidine- and Amino-Decorated Pores. *J. Am. Chem. Soc.* **132**, 38–39 (2010).
35. Si, X. L. *et al.* High and selective CO₂ uptake, H₂ storage and methanol sensing on the amine-decorated 12-connected MOF CAU-1. *Energy Environ. Sci.* **4**, 4522–4527 (2011).
36. Couck, S. *et al.* An Amine-Functionalized MIL-53 Metal–Organic Framework with Large Separation Power for CO₂ and CH₄. *J. Am. Chem. Soc.* **131**, 6326–6327 (2009).
37. Lu, W. *et al.* Sulfonate-Grafted Porous Polymer Networks for Preferential CO₂ Adsorption at Low Pressure. *J. Am. Chem. Soc.* **133**, 18126–18129 (2011).
38. Zhu, X. *et al.* Efficient CO₂ Capture by Porous, Nitrogen-Doped Carbonaceous Adsorbents Derived from Task-Specific Ionic Liquids. *Chem Sus Chem* **5**, 1912–1917 (2012).
39. Lassig, D. *et al.* A Microporous Copper Metal–Organic Framework with High H₂ and CO₂ Adsorption Capacity at Ambient Pressure. *Angew. Chem. Int. Ed.* **50**, 10344–10348 (2011).
40. Yang, S. J. *et al.* MOF-Derived Hierarchically Porous Carbon with Exceptional Porosity and Hydrogen Storage Capacity. *Chem. Mater.* **24**, 464–467 (2012).
41. Kim, C. *et al.* Fabrication of Electrospinning-Derived Carbon Nanofiber Webs for the Anode Material of Lithium-Ion Secondary Batteries. *Adv. Funct. Mater.* **16**, 2393–2397 (2006).
42. Price, B. K. & Tour, J. M. Functionalization of Single-Walled Carbon Nanotubes “On Water” *J. Am. Chem. Soc.* **128**, 12899–12904 (2006).
43. Dyke, C. A., Stewart, M. P., Maya, F. & Tour, J. M. Diazonium-Based Functionalization of Carbon Nanotubes: XPS and GC-MS Analysis and Mechanistic Implications. *SynLett*, 155–160 (2004).
44. Lillo-Rodenas, M. A., Cazorla-Amoros, D. & Linares-Solano, A. Understanding chemical reactions between carbons and NaOH and KOH An insight into the chemical activation mechanism. *Carbon* **41**, 267–275 (2003).
45. Zheng, S. T. *et al.* Pore Space Partition and Charge Separation in Cage-within-Cage Indium–Organic Frameworks with High CO₂ Uptake. *J. Am. Chem. Soc.* **132**, 17062–17064 (2010).
46. Yushin, G., Dash, R., Jagiello, J., Fischer, E. & Gogotsi, Y. Carbide-Derived Carbons: Effect of Pore Size on Hydrogen Uptake and Heat of Adsorption. *Adv. Funct. Mater.* **16**, 2288–2293 (2006).
47. Chen, Q. *et al.* Microporous Polycarbazole with High Specific Surface Area for Gas Storage and Separation. *J. Am. Chem. Soc.* **134**, 6084–6087 (2012).
48. Tan, Y.-X., Wang, F., Kang, Y. & Zhang, J. Dynamic Microporous indium(III)-4,4'-oxybis(benzoate) Framework with High Selectivity for the Adsorption of CO₂ over N₂. *Chem. Commun.* **47**, 770–772 (2011).
49. Jorda-Beneyto, M., Suarez-Garcia, F., Lozano-Castello, D., Cazorla-Amoros, D. & Linares-Solano, A. Hydrogen Storage on Chemically Activated Carbons and Carbon Nanomaterials at High Pressures. *Carbon* **43**, 293–303 (2007).
50. Wang, H.-L., Cao, Q.-M., Hu, J. & Chen, Z. High Performance of Nanoporous Carbon in Cryogenic Hydrogen Storage and Electrochemical Capacitance. *Carbon* **47**, 2259–2268 (2009).

Acknowledgments

This work was supported by the National Basic Research Program of China (2011CB808703, 2012CB821700), National Natural Science Foundation of China (Grant nos. 91022030, 21261130584), “111” project (B07016), Award Project of KAUST (CRG-1-2012-LAI-009) and Ministry of Education, Science and Technology Development Center Project (20120061130012).

Author contributions

T.B. and S.L.Q. designed the study. Y.Q.L. performed the experiments as well as most of the characteristics. B.Y.Z. measured the high pressure gas sorption. Y.F. carried out the TEM analysis. T.B. and Y.Q.L. prepared the manuscript and all authors reviewed the manuscript.

Additional information

Supplementary information accompanies this paper at <http://www.nature.com/scientificreports>

Competing financial interests: The authors declare no competing financial interests.

How to cite this article: Li, Y.Q., Ben, T., Zhang, B.Y., Fu, Y. & Qiu, S.L. Ultrahigh Gas Storage both at Low and High Pressures in KOH-Activated Carbonized Porous Aromatic Frameworks. *Sci. Rep.* **3**, 2420; DOI:10.1038/srep02420 (2013).



This work is licensed under a Creative Commons Attribution-NonCommercial-NoDerivs 3.0 Unported license. To view a copy of this license, visit <http://creativecommons.org/licenses/by-nc-nd/3.0>